Ethyl Thioglycolate Assisted Multifunctional Surface Modulation for Efficient and Stable Inverted Perovskite Solar Cells

Advanced Functional Materials

Wang, Yu; Wang, Feng; Song, Jiaxing; Ye, Jingchuan; Cao, Jieying et al

https://doi.org/10.1002/adfm.202402632

ADVANCED FUNCTIONAL MATERIALS
www.afm-journal.de

Ethyl Thioglycolate Assisted Multifunctional Surface Modulation for Efficient and Stable Inverted Perovskite Solar Cells

Yu Wang, Feng Wang, Jiaxing Song, Jingchuan Ye, Jieying Cao, Xinxing Yin, Zhen Su, Yingzhi Jin, Lin Hu, Han Zuilhof, Zaifang Li,* Wensheng Yan,* and Feng Gao*

As the core component of sandwich-like perovskite solar cells (PSCs), the quality of perovskite layer is a challenge for further progress in PSCs due to the unfavorable defects and uncontrollable crystallization. Here, a surface post-treatment strategy employing ethyl thioglycolate (ET) as ligand molecule is developed for property manipulation of perovskite films. ET can lower surface energy of perovskite facets and induces secondary growth of grains, giving films with higher crystallinity and lower defect density. Meanwhile, both carbonyl and sulfhydryl in ET can bind to the Pb^{2+}, thus forming bidentate anchoring on the surface for defect passivation. Besides, the perovskite/ET/C_{60} interface presents improved charge transfer owing to the well-aligned energy levels. Consequently, the power-conversion-efficiency (PCE) is boosted to 22.42% and 23.56% (certified 23.29%) for the $FA_{0.85}Cs_{0.15}Pb(I_{0.95}Br_{0.05})_3$ and $FA_{0.9}MA_{0.05}Cs_{0.05}Pb(I_{0.95}Br_{0.05})_3$ PSCs, respectively, and the $FA_{0.85}Cs_{0.15}Pb(I_{0.95}Br_{0.05})_3$-based PSC with a larger area (1.03 cm^2) delivers a PCE of 20.01%. Importantly, ET demonstrates effective management of I_2 and PbI_2, thereby preventing accelerated degradation and lead leakage of devices. Thanks to the multiple effects of ET, the resulting devices exhibit significantly enhanced ambient stability over a course of 800 h, and a thermal stability of over 1500 h while maintaining 80.4% of its original efficiency.

1. Introduction

The characteristics attributed to perovskite solar cells (PSCs) with facile fabrication process, rapidly growing power conversion efficiency (PCE), and their potential industrialization trend have been responsible for the considerable amount of attention from academia in the past decade.[1–5] Currently, the certified PCE for both single-junction PSCs with regular (*n–i–p*) and inverted (*p–i–n*) type exceeds 25%.[6–10] Compared to the former, inverted PSCs with a deposition sequence of hole-transport layer (HTL)/perovskite (PVK)/electron-transport layer (ETL) exhibit lower preparation energy consumption, better stability and broader application potential in the field of tandem or flexible photovoltaics.[11–14]

The PVK layer is the core in sandwich-like PSCs, which is involved in light harvesting, charge generation and separation, playing an important role in obtaining high-performance devices.[10,15] The lower crystallization energy barrier of polycrystalline PVK materials is beneficial for the flexibility in processing, but inevitably lead to a variety of defects in PVK bulk and at the surfaces and grain boundaries (GBs) during film processing and growth (e.g., crystallographic defects, point defects).[15–18] The existence of the high-density defects at PVK GBs and surfaces will induce severe nonradiative recombination losses through capturing carriers, and affect energy band alignment between the PVK/HTL or ETL interface causing the inefficient charge extraction, which greatly hampers the enhancement in PCE for PSCs.[19–21] In addition, the defects on PVK films tend to be preferred sites for disruption by external factors (e.g., oxygen, heat), providing pathways for migration or volatilization, which accelerates the degradation of PVK layer and the attenuation of photovoltaic parameters.[22–26] Therefore, the preparation of high-quality PVK films with large grain size, and lower GB and defect density is critical to achieving efficient and stable PSCs.

Additive strategies have been widely applied to synergistically regulate PVK crystallization and film defects to the point of obtaining high-quality PVK films, thus benefiting device performance.[27–31] For example, after introducing phenformin

Y. Wang, J. Song, J. Ye, J. Cao, X. Yin, Z. Su, Y. Jin, L. Hu, H. Zuilhof, Z. Li
China-Australia Institute for Advanced Materials and Manufacturing
College of Biological
Chemical Science and Engineering
Jiaxing University
Jiaxing 314001, China
E-mail: songjx@zjxu.edu.cn; zaifang.li@zjxu.edu.cn
Y. Wang, J. Ye, W. Yan
Institute of Carbon Neutrality and New Energy
School of Electronics and Information
Hangzhou Dianzi University
Hangzhou 310018, China
E-mail: wensheng.yan@hdu.edu.cn
F. Wang, F. Gao
Department of Physics
Chemistry and Biology (IFM)
Linköping University
Linköping 58183, Sweden

The ORCID identification number(s) for the author(s) of this article can be found under https://doi.org/10.1002/adfm.202402632

DOI: 10.1002/adfm.202402632

hydrochloride (PFCl) into PVK precursors, Zang et al. found that PFCl was able to not only facilitate the crystallization of PVK, but also passivate the multiple types of defects.[27] Similarly, Shi et al. demonstrated that the incorporation of 4-fluorophenethylammonium iodide (4-F-PEAI) could simultaneously optimize the crystallinity and interfacial defects of PVK.[28] Although the introduction of functional molecules into PVK can achieve the improvement of multifaceted properties of PVK, the PVK films with additives tend to become preferential degradation sites due to the presence of heterogeneous microstructures, which in turn is not conducive to the long-term retention of device performance.[32]

Currently, the post-treatment on top surface of PVK films based on the tuning of interfacial properties has become an effective and popular strategy to improve the performance of PSCs.[32–38] Liu et al. introduced histamine (HA) on the surface of inorganic PVK to control defects, prohibiting the nonradiative recombination within devices.[37] Zhu et al. introduced ferrocenyl-bis-thiophene-2-carboxylate ($FcTc_2$) into the PVK surface, which not only passivated the surface trap states but also inhibited the ionic migration of PVK.[12] The functional organic salts are also applied to modulate the terminal environment of PVK surface, resulting in the suppression of trap-assisted recombination.[38,39] Yang et al. showed a PVK post-treatment based on organic ammoniums as modifiers, which enables the secondary growth of grains, thus acquiring the high quality PVK films.[32] Besides, for slowing down the damage of I^- generated from the PVK on the device performance, Fang et al. effectively enhanced the device stability after introducing trimethylolpropane triacrylate (TMTA) to the PVK surface.[40] However, it is still a great challenge to simultaneously realize crystallization modulation, defect passivation, and decomposition products management of PVKs by employing one passivation molecule based on the surface treatment.

Noticeably, the intrinsic "soft"-structured halide PVKs with both crystalline solid and liquid-like behaviors has been demonstrated to offer the possibility of regulating their thin film recrystallization via a simple tuning of surface features.[32,41,42] Besides, it should be further pointed out that PVK is prone to producing decomposition products of PbI_2 and I_2 during device operation, which provides additional channels for PVK decomposition and electrode damage, accelerating device degradation.[26] Hence, effective management of I_2 and PbI_2 at the interface by post-treatment is as essential to the performance improvement of PSCs as the acquisition of low defect and high crystallinity PVK films.

Compared to the organic and inorganic salts, the non-ionic organic modifiers without mobile ions may provide potential assistance toward the stable passivation and device long-term stability. To establish the surface chemical interaction and tune the properties of PVKs, appropriate functional groups as electron donors or acceptors are usually incorporated into the modifier molecules.[43–46] For instance, the carbonyl (carboxyl and amide) or sulfhydryl have been widely demonstrated to interact with the undercoordinated Pb^{2+} by Lewis base-acid reaction.[47–50] Particularly, the multiple-active-site organic molecules with multiple functional groups typically have strong synergistic effects, which should be developed to maximize their modulation potentials for PVKs.[50–52] Amongst, the ethyl thioglycolate (ET) molecule possesses two electron-donating functional groups, both sulfhydryl (-SH) and carbonyl (C═O), which can coordinate with Pb^{2+} in PVKs strongly (that is, show excellent reducing property).[50] ET based molecules with powerful PVK interactions are highly expected for achieving multifunctional surface modulation of PVKs, and it is highly desirable to achieve crystal growth modulation, defect passivation, and interfacial I_2 and PbI_2 management simultaneously by developing rational multifunctional ligand molecules.

Herein, we demonstrate a surface treatment strategy for property manipulation of PVK films based on ET, resulting in well-performing photovoltaic devices (Figure S1 and Table S1, Supporting Information). Theoretical calculations show that ET can lower the surface energy of the crystal planes of PVK and generate a driving force for the secondary growth of grains, leading to PVK films with larger grain sizes, higher crystallinity, and lower residual stress. Moreover, the uncoordinated Pb^{2+} on the surface of PVK film can be simultaneously anchored by R—C═O and R-SH in the ET, achieving a stable and efficient defect passivation. In addition, the introduction of ET enables a more favorable energy band alignment at the PVK//ETL interface, promoting the electron extraction and transport. Remarkably, the ET-treated devices exhibit excellent capture of I_2 and PbI_2 due to the strong electron-donating ability of ET, impeding the damage to PVK films and electrodes. As a result, the ET-treated PSCs based on $FA_{0.85}Cs_{0.15}Pb(I_{0.95}Br_{0.05})_3$ (FACs) and $FA_{0.9}MA_{0.05}Cs_{0.05}Pb(I_{0.95}Br_{0.05})_3$ (FAMACs) yield a champion PCE of 22.42% and 23.56% (certified 23.29%), respectively, and a PCE of 20.01% was achieved for the FACs-based PSC with a larger area of 1.03 cm^2. Also, the unencapsulated devices with ET exhibit a striking enhancement in stability after long-term storage in nitrogen, as well as under ambient air and thermal stress conditions. This facile, cost-effective and scalable post-treatment technology may provide support for the development of high-performance inverted PSCs for industrial application.

2. Results and Discussion

As shown in **Figure 1a**, an isopropanol (IPA) dissolved ethyl thioglycolate (ET) solution was spin-coated on the PVK film surface and the PVK/ET film was received after re-annealing treatment (100 °C, 5 min). To reveal the difference in properties of PVK films before and after ET modification, the results of multiple analyses for a comprehensive description were performed. In the following section, the PVK without and with ET treatment will be denoted as "control" and "target". First, the effect of ET on the surface morphology of PVK films were studied using scanning electron microscope (SEM) and atomic force microscopy (AFM). As presented in Figure 1b, the SEM images obtained from three different batches of samples consistently indicate that there is a significant increase in grain size for the target films, and the average grain size has doubled from 174.8 to 357.4 nm (Figure S2a, Supporting Information). The lower magnification SEM images at 1 µm scale are shown in Figure S3 (Supporting Information). Meanwhile, the cross-sectional SEM images also demonstrate that the target films have larger size and denser arrangement of grains (Figure 1b). Besides, the X-ray diffraction (XRD) patterns of the PVK films was obtained (the diffraction peaks at 14.1°, 19.9°, 24.5°, 28.3° and 31.7° were corresponding to the (100), (110), (111), (200) and (210) PVK crystal

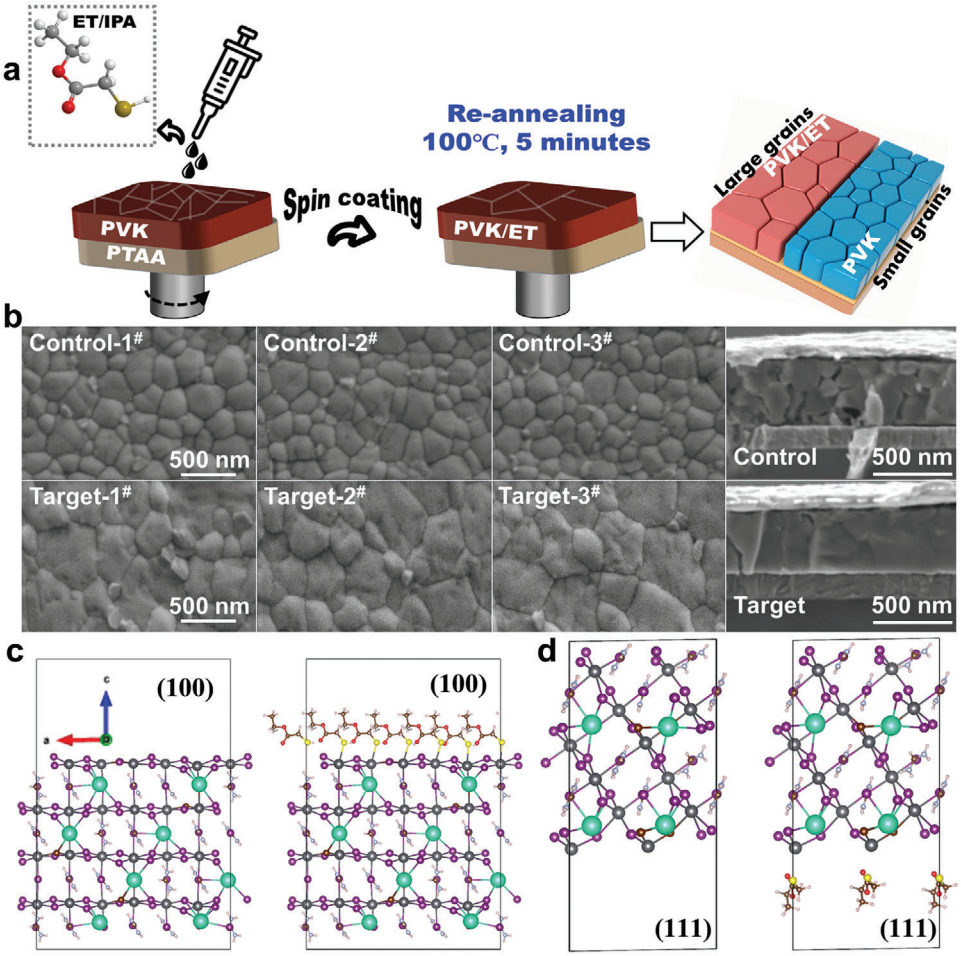

Figure 1. a) Illustration of ET modified PVK. b) Top-view and cross-sectional SEM images of control and target films. Optimized c) (100) and d) (111) slab model of FACs-based PVKs without (control) and with (target) ET treatment.

planes, respectively),[43] the target films exhibited the much stronger intensity than that of the control films, and the full width at half maximum (FWHM) of the main diffraction peaks for the target films presented smaller values, suggesting the crystallinity was enhanced after ET-treatment (Figure S2b, Supporting Information).[43,53] In order to exclude the effect of IPA, the top-view SEM of PVK films after treatment with pure-IPA was measured. As shown in Figure S4a (Supporting Information), it is found that there is no significant change in PVK grain size before and after pure-IPA treatment. Besides, from Figure S4b–d (Supporting Information), it can be analyzed that the bright flaky distributed on the surface of the PVK film are PbI_2 and the average size of the PVK grains after IPA washing is 162.3 nm. Hence, the increased grain size can be attributed to the introduction of ET on the PVK surface. To further clarify the origin of ET promoting the growth of PVK crystals, we used the density functional theory (DFT) to examine the difference in the surface energy of PVK grains before and after ET modification. Given the dominance of the (100) and (111) planes in the PVK crystal growth and the resulting optoelectronic properties of PVK thin films,[54] hence these two low-index planes were primarily considered. Theoretical calculations revealed that compared to the control PVK, the surface energy is remarkably reduced at both the ET-terminated (100) and (111) planes (Figure 1c; Table S2, Supporting Information), and the surface energy difference between (100) and (111) planes is −2.23 and −2.33 eV nm^{-2} for the control and target PVK, respectively. Therefore, there is an increasing surface energy anisotropy, which can provide a driving force to induce the secondary grain growth of the ET-treated PVK film, so that the grains will grow larger along the orientation that minimizes the free energy of the system.[55] The significantly enhanced (100) peak intensity in the XRD is consistent with the computational result that the (100) plane is more energy favorable after ET treatment. As displayed in the UV–vis absorption spectra of multiple samples (Figure S2c,d, Supporting Information), the absorption of the PVK film treated with ET was increased owing to the improved grain size and higher crystallinity[29]. Moreover, the surface morphology of PVK films is further studied using atomic force microscope (AFM), and the results indicate that the surface roughness of the PVK film dropped from 20.8 to 19.1 nm (Figure S2e,f), indicating the ET-driven sample has a smoother surface after secondary crystallization.

The ultraviolet photoelectron spectroscopy (UPS) results show that the conduction band minimum (CBM) of PVK film moves

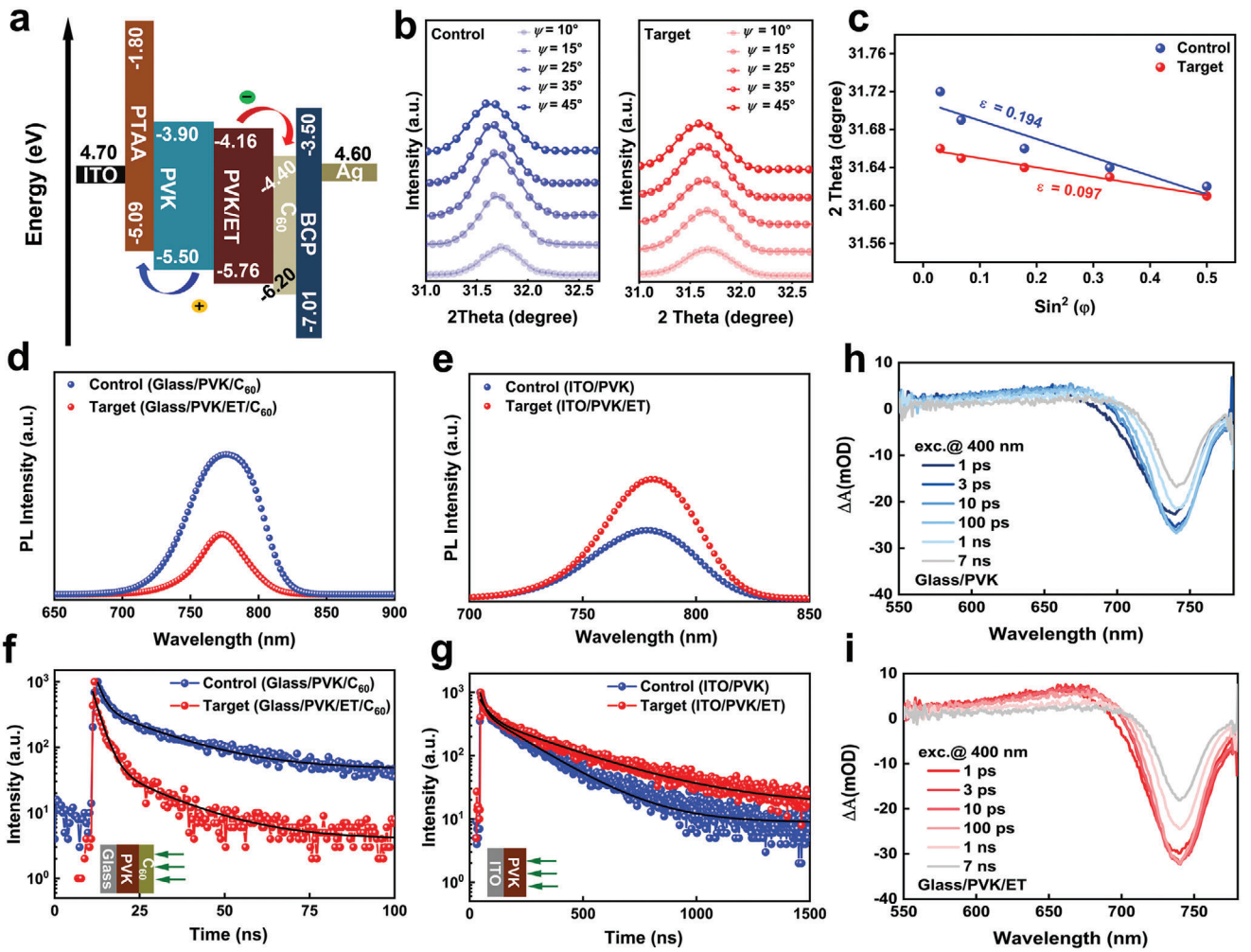

Figure 2. a) Schematic energy level alignment of ITO/PTAA/PVK without or with ET /C_{60}/BCP/Ag. b) The GIXRD with different ψ angles (from 10° to 45°) in the depth of ≈100 nm. c) Linear fit of 2θ-$\sin^2(\psi)$ based on control and target film. d,e) Steady-state PL spectra and f,g) TRPL decay curves of control and target PVK films deposited on various substrates. TA spectra at different delay times of h) control and i) target film.

from −3.90 to −4.16 eV after ET treatment, which is closer to the LUMO of C_{60} (−4.40 eV) (**Figure 2a**). The better energy level alignment at the PVK/C_{60} interface is beneficial for charge extraction and transport.[56–58] The calculated energy level parameters for control/target PVK films are listed in Table S3 (Supporting Information), which is derived from the Tauc-plots and energy cut-off ($E_{cut\text{-}off}$) and energy onset ($E_{on\text{-}set}$) regions of UPS (Figure S5, Supporting Information). To evaluate the difference in residual stress (ϵ) of PVK films before and after the ET-induced secondary grain growth, a series of grazing incident X-ray diffraction (GIXRD) patterns were conducted. The alternative of the (210) plane is more feasible than the (110) plane as it can reliably display the detailed grain information and attenuate the effect of orientation on the 2θ-$\sin^2\psi$.[59,60] Figure 2b shows the diffraction signals of control and target films at different ψ values. The fitting lines of 2θ-$\sin^2(\psi)$ reveal (Figure 2c) that the target PVK film has a lower slope value (0.097) than that of control film (0.194), indicating that the residual stress in the PVK film after secondary grain growth is released, which in turn favors the lattice-matched and stable PVK films. Furthermore, it has been observed a decrease in stress of PVK films contributes to an increase in the defect formation energy,[61,62] thus promoting a reduction in trap-assisted recombination. Then, the steady-state PL and time-resolved photoluminescence (TRPL) were employed to investigate the charge carrier dynamics occurring on different samples. As displayed in Figure 2d,f, the Glass/PVK/ET/C_{60} film exhibits lower steady-state PL intensity and faster PL decay, respectively, which suggests an effective charge transfer between the PVK/C_{60} interfaces, mainly due to the more matched energy bands at the interfaces.[41,61] Instead, a stronger PL signal and longer carrier lifetime (τ_{ave}) were observed for the target film composed of ITO/PVK/ET (Figure 2e,g), which confirms that the ET-treated PVK film has the lower non-radiative recombination loss, possibly attributed to the reduction of defects within the PVK film bulk and at the surface.[63] Tables S4 and S5 (Supporting Information) summarize the lifetime parameters characterized by the doubled-exponential decay function (Supporting Information for details). Furthermore, the transient absorption (TA) spectra revealed that there was the lower quenching rate of GSBS (ground state bleaching signal) for the target samples

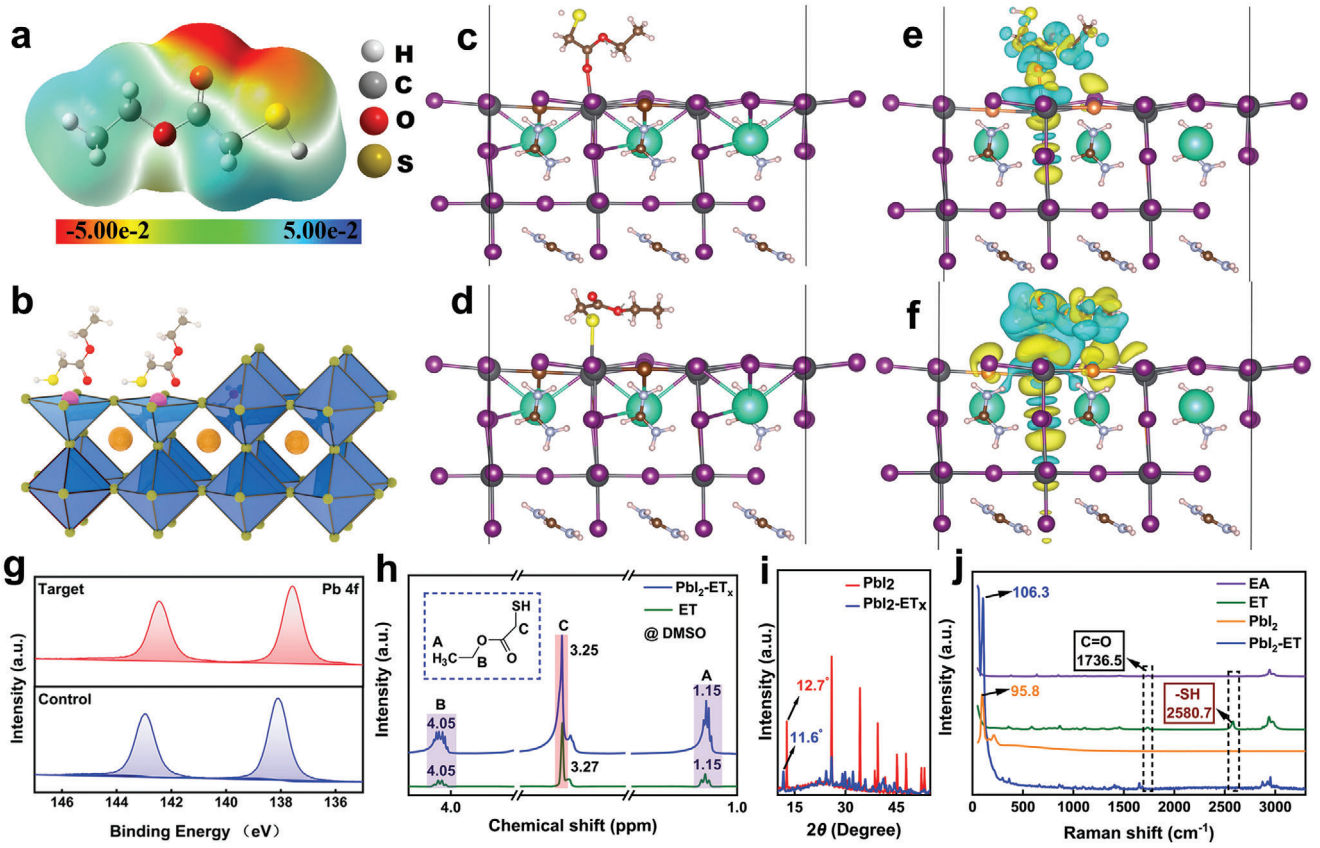

Figure 3. a) Electrostatic potential of ET. b) Schematic illustration of the chemical bridge between the ET and Pb^{2+}. Theoretical models of surface interaction of Pb^{2+} traps in the PVKs with c) carbonyl (R—C=O) and d) sulfydryl (R-SH) in the ET. Differential charge density distribution of the optimized surface structure of the PVKs interacted with e) carbonyl and f) sulfydryl. g) XPS of Pb 4f for control and target films. h) ^{1}H-NMR spectra of ET and PbI_2-ET. i) XRD patterns of PbI_2 and PbI_2-ET. j) Raman spectra of different samples.

(Figure 2h,i; the pseudo-color plots shown in Figure S6, Supporting Information), further demonstrating the suppressed non-radiative recombination after introducing ET on the PVK films.

In order to elucidate the potential chemical interaction between PVK and ET molecules, a variety of characterizations were conducted. As shown in **Figure 3a**, the computed electrostatic potential (ESP) diagrams by DFT (Density functional theory) indicate that the carbonyl (R—C=O) and sulfydryl (R-SH) in the ET have higher electron density (red region). Accordingly, the ET with these two functional groups can act as Lewis-base to coordinate with the uncoordinated Pb^{2+} by donating electrons (Figure 3b), thus suppressing the formation of defects appearing on the PVK surface. DFT calculations demonstrated that the binding energy (BE) values between R—C=O/R-SH and Pb were −0.27 and -0.30 eV, respectively, indicating that both functional groups can bind to uncoordinated Pb^{2+} while the sulfhydryl shows stronger binding ability (Figure 3c,d). Furthermore, the variation in charge density of the configurations was calculated to further visualize the interaction. Figure 3e,f suggests that the electron accumulation (yellow region) and hole accumulation (cyan region) are separated, which are present not only at the termination end but also extending deep inside of PVK film, mainly attributing to the strong binding between ET and PVKs.[64] The X-ray photoelectron spectroscopy (XPS) showed that the BE peaks of Pb 4f for the ET-treated PVK shifted from 142.95 and 138.08 eV to 142.46 and 137.59 eV, respectively, validating the chemical interaction between ET and PVKs (Figure 3g). Notably, as compared to the control film, a significant S signal from XPS was detected on the surface of target film, which indicated that the ET can still anchor on the PVK surface stably after the secondary annealing of PVK/ET film (Figure S7, Supporting Information). According to the ^{1}H nuclear magnetic resonance spectroscopy (^{1}H-NMR) shown in Figure 3h (the original spectrum is shown in Figure S8, Supporting Information), the proton signal corresponding to the position C of ET molecule shifted from the 3.27 to 3.25 ppm for the PbI_2-ET solution, suggesting the presence of bonding interaction between Pb^{2+} and the carbonyl/sulfhydryl groups in ET, in agreement with the XPS analysis. To further reveal the binding mode of the functional groups in the ET molecule with Pb^{2+}, we successfully prepared the PbI_2-ET complex (Figure S9a, Supporting Information), and then measured the XRD pattern. It found that the diffraction peak of PbI_2 at 12.7° completely disappeared in the PbI_2-ET complex sample, accompanied by an emerging diffraction signal of the new compound at 11.6°, indicating the strong and irreversible binding of ET and PbI_2 (Figure 3i). Meanwhile, the thermogravimetry analysis (TGA) exhibited that the above complexes could be stabilized within ≈110 °C, again proving that the PVK/ET films were able to achieve an effective

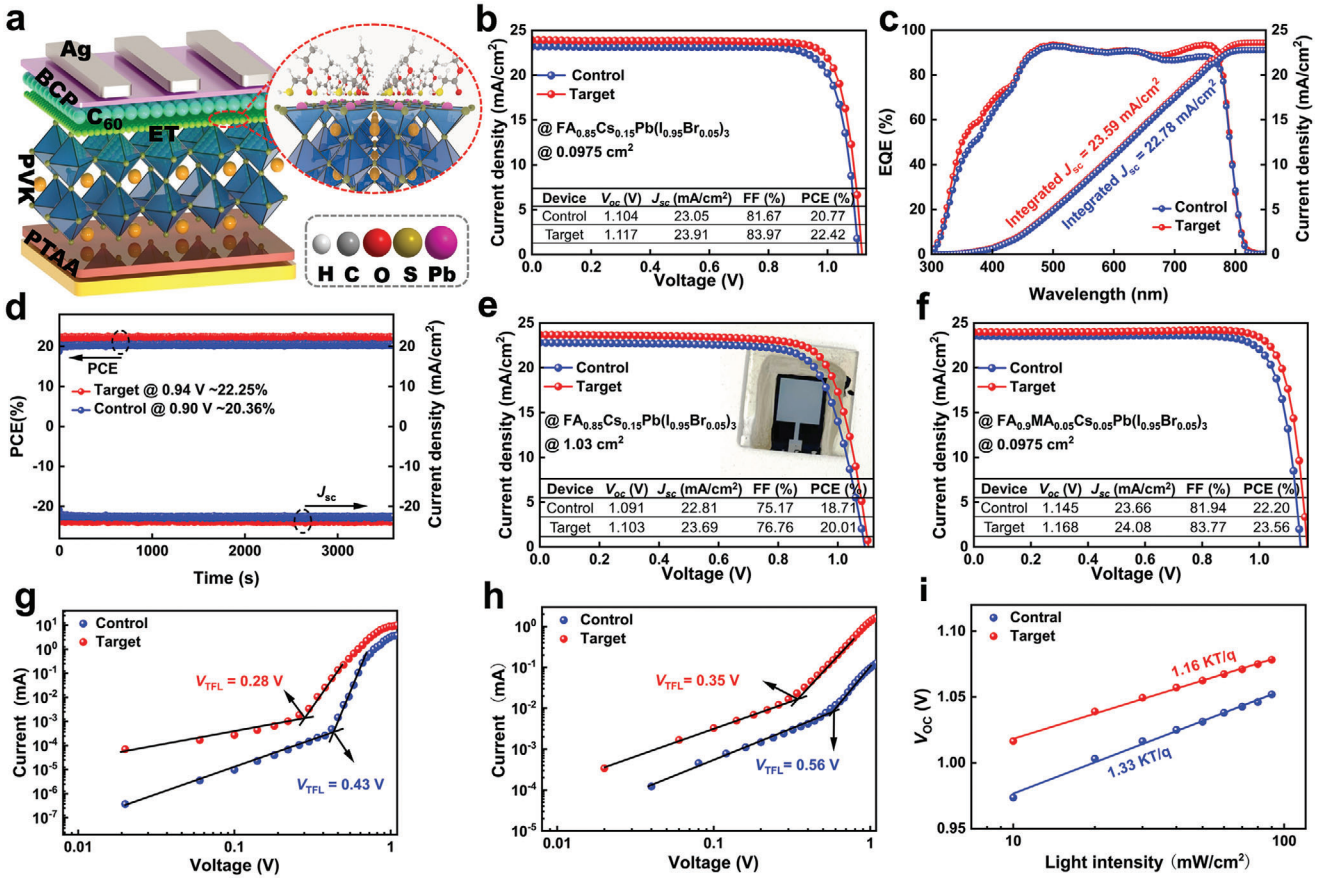

Figure 4. a) The device structure of ET-treated PSCs (ITO/HTL/PVKs/ET/C_{60}/BCP/Ag). b) Photocurrent density–voltage (*J–V*) curves and c) EQE spectra of FACs-based PSCs with an active area of 0.0975 cm^2. d) Steady state output of control and target device. *J–V* curves of e) FACs-PSCs with an active area of 1.03 cm^2) and f) FAMACs-PSCs with an active area of 0.0975 cm^2. Dark *I–V* curves for the g) electron-only (ITO/PVK/C_{60}/Ag) and h) hole-only (ITO/PTAA/PVK/MoO_3/Au) devices based on the control and target PVKs. i) V_{oc} versus light intensity for the control and target PSCs.

attachment of ET after treatment at 100 °C (Figure S9b, Supporting Information). In addition, we analyzed the Raman spectra of the different liquid samples based on the quartz/Ag substrate. As presented in Figure 3j and Figure S10a (Supporting Information), ET showed significant Raman signals at 2580 and 1736 cm^{-1}, and by comparing the Raman data of ethyl acetate (EA), it can be analyzed that these two signals belonged to the sulfhydryl and carbonyl groups in ET, respectively.[65] However, for PbI_2-ET powder, the characteristic signal of carbonyl group appeared at ≈1700 cm^{-1}, while that of sulfhydryl group almost disappeared, along with a new signal emerging at ≈106 cm^{-1} (Figure 3j; Figure S10b, Supporting Information), indicating that the carbonyl and sulfhydryl can bind to Pb^{2+} and the sulfhydryl group exhibits a stronger binding ability. Noteworthily, with increasing PbI_2, the Raman signal of sulfhydryl in the ET+PbI_2/DMF samples experienced a regular weakening until it almost disappeared, as shown in Figure S10c (Supporting Information). This again demonstrated the sensitive and powerful binding between sulfhydryl in ET and Pb^{2+}. Therefore, based on the above theoretical and experimental analyses, it can be concluded that both carbonyl and sulfhydryl groups in ET can bind to the uncoordinated Pb^{2+}, thus potentially forming bidentate anchoring on the surface of PVK for passivation, and the strong interaction between ET and PVK drives the reduction of surface energies of the crystal planes, leading to the secondary growth and thus high crystallinity of PVK grains.

To evaluate the difference in photovoltaic (PV) performance of the devices without (control) and with (target) ET treatment, the planar inverted PSCs with the structure of ITO/PTAA/PVK/with or without ET/C_{60}/BCP/Ag were developed (**Figure 4a**). As shown in Figure 4b, the target device exhibit the champion PCE of 22.42% with a short-circuit current density (J_{sc}) of 23.91 mA cm^{-2}, an open-circuit voltage (V_{oc}) of 1.117 V, and a fill factor (FF) of 83.97%, which is superior to the optimum control device with a PCE of 20.77% (J_{sc} of 23.05 mA cm^{-2}, V_{oc} of 1.104 V, and FF of 81.67%). Particularly, the significantly improved average values of the PV parameters were yielded for the target device (Table S6, Supporting Information) that could be mainly attributed to the enhanced quality of the PVK film with high crystallinity and reduced defects, and the favorable interfacial energy band modulation, as elucidated above. The PV parameters (i.e., PCE, V_{oc}, J_{sc}, FF) statistics of the control and target devices are shown in Figure S11a (Supporting Information). The external quantum efficiency (EQE) results (Figure 4c) revealed the integral currents of 22.78 and 23.59 mA cm^{-2} for the control and target devices, respectively, agreeing well with the achieved

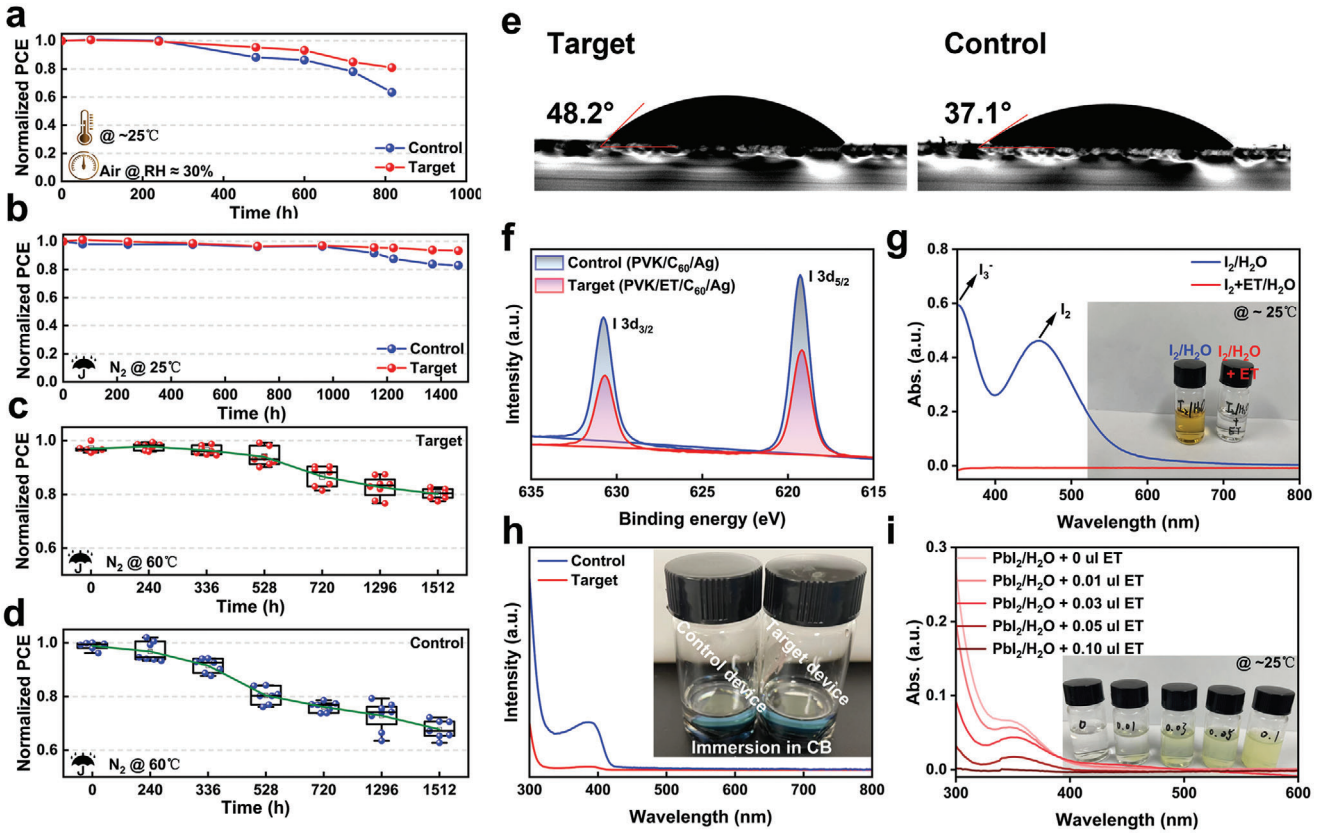

Figure 5. Normalized PCE decay of FACs-based PSCs without (control) or with (target) ET treatment stored in a) ambient air, b) N_2 at room temperature, and c,d) N_2 at 60 °C,. e) Water contact angle measurements of control and target films. f) XPS of I 3d for control and target samples after accelerated aging (continuous light and heating at 80 °C ≈10 days). UV–vis absorption of g) I_2/H_2O and i) PbI_2/H_2O without or with ET, h) UV–vis absorption of the solution after immersion of the control and target devices in chlorobenzene (CB) for two weeks.

J_{sc} values by the current–voltage (J–V) test. In addition, the steady power output tests within 1 h showed that the target device exhibited a more efficient and stable PCE output compared to the control one (Figure 4d). Meanwhile, the high-performance PSC devices with large-area (1.03 cm^2) were successfully fabricated. As illustrated in Figure 4e, the champion PCE of the FACs-based PSC has been elevated to over 20% after ET modification (the PV parameters and statistics are shown in Table S7 and Figure S11b (Supporting Information)), demonstrating the scalability of the ET treatment process and showing its potential for large-scale manufacturing. Notably, we have successfully applied the interface strategy of ET processing to the fabrication of FAMACs-based PSCs, and the significantly increased PCE from 22.20% to 23.56% (certified 23.29%, Figure S12, Supporting Information) has been obtained for the triple-cation PSCs (Figure 4f). The detailed PV parameters and statistics see Table S8 and Figure S11c (Supporting Information), respectively. The steady power output and EQE spectrum are shown in Figure S13 (Supporting Information). All excellent device performances have demonstrated the universality of interface strategy based on ET functional molecule in enhancing PV performance of PSCs.

To better understand the charge recombination characteristics of devices, the dark-current measurement of devices was carried out. As illustrated in Figure S14a (Supporting Information), there is the lower leakage current density for the target device, indicating that the charge carriers of the target device are more prone to be extracted than recombined. Further, we quantified the differences in the defects of PVK films before and after introducing ET based on the popular space-charge limited current (SCLC) technique (Supporting Information for details).[63] As shown in Figure 4g,h, the trap filled limit voltage (V_{TFL}) and calculated trap densities (N_{trap}) of the target devices are 0.28 V and 2.70×10^{15} cm^{-3} (electron-only), 0.35 V and 3.41×10^{15} cm^{-3} (hole-only), respectively, which are lower than the values of control electron-only (V_{TFL} = 0.43 V, $N_{trap} = 4.22 \times 10^{15}$ cm^{-3}) and hole-only devices (V_{TFL} = 0.56 V, $N_{trap} = 5.50 \times 10^{15}$ cm^{-3}). In terms of the light intensity dependent V_{oc} results (Figure 4i), the target device possessed a smaller slope of 1.16 kT q^{-1} with respect to the control one (1.33 kT q^{-1}), signifying that the trap-assisted recombination was suppressed. In addition, the electrochemical impedance spectroscopy (EIS) showed that a lower R_s (series resistance) but higher R_{rec} (recombination resistance) was simultaneously produced for the target device (Figure S14b, Supporting Information), indicative of the improved charge extraction and transport at the PVK/ET/C_{60} interface. In brief, these results proved that ET could effectively reduce the defects of PVKs through surface passivation and induced crystallization regulation, thus suppressing the non-radiative recombination and promoting transport of charges.

Not only does the PCE significantly benefit from the ET treatment, but also the stability shows remarkable boost. As illustrated in **Figure 5**, the unencapsulated target device exhibited 81% and 93% PCE retention after aging in air (Figure 5a) and nitrogen (Figure 5b) for ≈800 and ≈1400 h, respectively, while the PCE of the control device decayed at a higher rate (i.e., the control device stays 60% and 81% of the initial PCE under the same aging conditions). The evolution trends of the detailed PV parameters are shown in Figure S15 (Supporting Information). It is noteworthy that after aging at 60 °C for more than 1500 h, the average PCE of the target device still maintained 80.4% of the initial value (Figure 5c,d). whereas the PCE of the control device was only 67.8% of the initial value. Figure S16 (Supporting Information) shows the decay trends of the relevant PV parameters. In addition to the effective defect passivation and crystallization quality control for PVK with the introduction of ET, the increased hydrophobicity of the PVK/ET surface may partly facilitate the elevated stability of target device (Figure 5e). Additionally, the MPP (maximum power point) tracking results for the control and target device are provided in Figure S17 (Supporting Information). The normalized PCE of the control device decayed significantly after ≈600 h, retaining only ≈80% of the initial PCE value, whereas the ET-treated target device still maintained ≈93%.

It is widely known that long-term storage of PSCs at high temperature can easily induce decomposition of PVK to produce PbI_2 and I_2.[66,67] Besides, the unbonded I^- present on the PVK surface traps holes and thus generates highly corrosive I_2 (Although the accumulated charges at the PVK/ETL interface would make the I^- relatively stable, there are still a minor amount of holes trapped by I^- at the interface, forming I_2).[26] The diffusion of I_2 will accelerate the corrosion of metal electrodes, which in turn affects the device performance. As presented in Figure 5f, we examined the XPS of control/target samples after accelerated aging (i.e., continuous light and heating at 80 °C) for 10 days. The peaks located at 619.27 eV (control) and 619.22 eV (target) are all corresponding to the I^- derived from AgI, indicating that the devices suffered from I_2 erosion during aging.[40,46] However, the XPS signal of I^- for the target film was significantly weaker than the control one, disclosing that the erosion rate of Ag electrodes by I_2 in the PVK/ET/C_{60}/Ag was markedly inhibited. Figure 5g illustrates the UV–vis absorption peaks of the I_2/H_2O are located near 350 and 450 nm, assigned to the characteristic signals of I_3^- and I_2, respectively.[22,31] With the addition of ET, the absorption peaks disappeared visibly, indicating that ET could capture I_2 (i.e., the reduction of I_2 by ET) quickly and effectively (Video S1, Supporting Information). Therefore, the inhibited generation of I_2 originating from the introduction of ET on the PVK surface can greatly slow down the degeneration of PVKs and electrodes, thereby improving the stability of PSC device.[26,46] Furthermore, interestingly, it was found that the absorption intensity of PbI_2/H_2O solution gradually diminished with increasing ET at room temperature (Figure 5i), suggesting that ET has a strong capacity to capture PbI_2, which is in accordance with the analysis of Figure S10c (Supporting Information). A comparison of UV–vis absorption of the solutions obtained after immersing the devices in chlorobenzene (CB) for two weeks revealed that the target solution exhibited a significantly weakened PbI_2 characteristic signal compared to the control one (Figure 5h), further indicative of a decent PbI_2 management capability of the ET-processed devices, thereby obstructing lead leakage and the channels for PVK degeneration. It can be seen that the use of low-cost ET combined with the simple surface modification strategy can provide support and guidance for solving the long-term stability and environmental unfriendly problems faced by PSCs in the industrialization process.

3. Conclusion

In summary, we developed a surface engineering by ethyl thioglycolate modification to improve the performance of inverted PSCs, delivering an increased PCE to 22.42% and 23.56% for the target FACs- and FAMACs-based device, respectively. Besides, the FACs-based device with a larger area (1.03 cm^2) yielded a highest PCE of 20.01% after ET processing. Attributable to the following merits: i) the defects present at PVK surface are effectively passivated through the bidentate anchoring of R—C═O and R-SH in ET with undercoordinated Pb^{2+} in PVKs; ii) the secondary grain growth of surface PVK is induced by ET, owing to the reduced surface energy of crystal planes that provides a growth driving force, resulting in films with larger grain size and low GBs; iii) ET-treated PVK/C_{60} interface exhibits a more matched energy level, thus enabling more efficient charge transfer at the interface. Besides, ET demonstrated the strong capacity to capture I_2 and PbI_2, preventing the degradation of PVKs and decay of PV performance. With the help of multiple effects of ET, the unencapsulated target devices exhibited excellent ambient and long-term stability after storage in air and N_2, respectively, and the average PCE of target device can still keep 80.4% of the initial value even after aging at 60 °C for more than 1500 h.

Supporting Information

Supporting Information is available from the Wiley Online Library or from the author.

Acknowledgements

This research was supported by the Zhejiang Provincial Natural Science Foundation of China (Nos. LQ23E030005, LGJ22B040001, KYZ044123045CZ), the Jiaxing Public Welfare Research Project (No. 2022AY10003), the Zhejiang Provincial Postdoctoral Science Foundation (No. ZJ2022148), the Innovation Jiaxing·Elite leading plan 2020, the National Key Research and Development Program of China (Grant No. 2022YFB4200904).

Conflict of Interest

The authors declare no conflict of interest.

Data Availability Statement

The data that support the findings of this study are available from the corresponding author upon reasonable request.

Keywords

ethyl thioglycolate, inverted perovskite solar cells, secondary crystallization, stability, surface passivation

Received: February 12, 2024
Revised: May 17, 2024
Published online:

[1] A. Kojima, K. Teshima, Y. Shirai, T. Miyasaka, *J. Am. Chem. Soc.* **2009**, *131*, 6050.
[2] Y. Zhao, F. Ma, Z. Qu, S. Yu, T. Shen, H.-X. Deng, X. Chu, X. Peng, Y. Yuan, X. Zhang, J. You, *Science* **2022**, *377*, 531.
[3] M. Kim, J. Jeong, H. Lu, K. Lee Tae, T. Eickemeyer Felix, Y. Liu, W. Choi In, J. Choi Seung, Y. Jo, H.-B. Kim, S.-I. Mo, Y.-K. Kim, H. Lee, G. An Na, S. Cho, R. Tress Wolfgang, M. Zakeeruddin Shaik, A. Hagfeldt, Y. Kim Jin, M. Grätzel, S. Kim Dong, *Science* **2022**, *375*, 302.
[4] Y. J. Luo, K. K. Liu, L. Yang, W. J. Feng, L. F. Zheng, L. Shen, Y. B. Jin, Z. Fang, P. Q. Song, W. J. Tian, P. Xu, Y. Q. Li, C. B. Tian, L. Q. Xie, Z. H. Wei, *Nat. Commun.* **2023**, *14*, 3738.
[5] R. He, W. H. Wang, Z. J. Yi, F. Lang, C. Chen, J. C. Luo, J. W. Zhu, J. Thiesbrummel, S. Shah, K. Wei, Y. Luo, C. L. Wang, H. G. Lai, H. Huang, J. Zhou, B. S. Zou, X. X. Yin, S. Q. Ren, X. Hao, L. L. Wu, J. Q. Zhang, J. B. Zhang, M. Stolterfoht, F. Fu, W. H. Tang, D. W. Zhao, *Nature* **2023**, *618*, 80.
[6] H. Min, D. Y. Lee, J. Kim, G. Kim, K. S. Lee, J. Kim, M. J. Paik, Y. K. Kim, K. S. Kim, M. G. Kim, T. J. Shin, S. I. Seok, *Nature* **2021**, *598*, 444.
[7] Z. Liang, Y. Zhang, H. F. Xu, W. J. Chen, B. Y. Liu, J. Y. Zhang, H. Zhang, Z. H. Wang, D.-H. Kang, J. R. Zeng, X. Y. Gao, Q. S. Wang, H. J. Hu, H. M. Zhou, X. B. Cai, X. Y. Tian, P. Reiss, B. M. Xu, T. Kirchartz, Z. G. Xiao, S. Y. Dai, N.-G. Park, J. J. Ye, X. Pan, *Nature* **2023**.
[8] National Renewable Energy Laboratory (NREL), Photovoltaic Research, Best Research-Cell Efficiency Chart, https://www.nrel.gov/pv/cell-efficiency.html, (accessed: September 2023).
[9] G. Yang, Z. W. Ren, K. Liu, M. C. Qin, W. Y. Deng, H. K. Zhang, H. B. Wang, J. W. Liang, F. H. Ye, Q. Liang, H. Yin, Y. X. Chen, Y. L. Zhuang, S. Q. Li, B. W. Gao, J. B. Wang, T. T. Shi, X. Wang, X. H. Lu, H. B. Wu, J. H. Hou, D. Y. Lei, S. K. So, Y. g. Yang, G. J. Fang, G. Li, *Nat. Photonics* **2021**, *15*, 681.
[10] S. Zhang, F. Y. Ye, X. Y. Wang, R. Chen, H. D. Zhang, L. Q. Zhan, X. Y. Jiang, Y. W. Li, X. Y. Ji, S. J. Liu, M. J. Yu, F. R. Yu, Y. L. Zhang, R. H. Wu, Z. H. Liu, Z. J. Ning, D. Neher, L. Y. Han, Y. Z. Lin, H. Tian, W. Chen, M. Stolterfoht, L. J. Zhang, W.-H. Zhu, Y. Z. Wu, *Science* **2023**, *380*, 404.
[11] N. Li, X. Niu, Q. Chen, H. Zhou, *Chem. Soc. Rev.* **2020**, *49*, 8235.
[12] Z. Li, B. Li, X. Wu, S. Sheppard, S. Zhang, D. Gao, N. J. Long, Z. L. Zhu, *Science* **2022**, *376*, 416.
[13] S. F. Wu, J. Zhang, Z. Li, D. J. Liu, M. C. Qin, S. H. Cheung, X. H. Lu, D. Y. Lei, S. K. So, Z. L. Zhu, A. K.-Y. Jen, *Joule* **2020**, *4*, 1248.
[14] Q. Jiang, Y. Zhao, X. Zhang, X. Yang, Y. Chen, Z. Chu, Q. Ye, X. Li, Z. Yin, J. You, *Nat. Photonics* **2019**, *13*, 460466.
[15] M. G. Li, Z. Zhu, Z. Z. Wang, W. J. Pan, X. X. Cao, G. B. Wu, R. F. Chen, *Adv. Mater.* **2024**, *36*, 2309428.
[16] J. W. Lee, H. Yu, K. Lee, S. Bae, J. Kim, G. R. Han, D. Hwang, S. K. Kim, J. Jang, *J. Am. Chem. Soc.* **2019**, *141*, 5808.
[17] D. T. Moore, H. Sai, K. W. Tan, D. M. Smilgies, W. Zhang, H. J. Snaith, U. Wiesner, L. A. Estroff, *J. Am. Chem. Soc.* **2015**, *137*, 2350.
[18] M. Degani, Q. Z. An, M. Albaladejo-Siguan, Y. J. Hofstetter, C. Cho, F. Paulus, G. Grancini, Y. Vaynzof, *Sci. Adv.* **2021**, *7*, eabj7930.
[19] N. Li, S. Tao, Y. Chen, X. Niu, C. Onwudinanti, C. Hu, Z. Qiu, Z. Xu, G. Zheng, L. Wang, Y. Zhang, L. Li, H. Liu, Y. Lun, J. Hong, X. Wang, Y. Liu, H. Xie, Y. Gao, Y. Bai, S. Yang, G. Brocks, Q. C. H. Zhou, *Nat. Energy* **2019**, *4*, 408.
[20] J. Xu, H. Dong, J. Xi, Y. G. Yang, Y. Yu, L. Ma, J. B. Chen, B. Jiao, X. Hou, J. R. Li, Z. X. Wu, *Nano Energy* **2020**, *75*, 104940.
[21] A. R. b. Mohd Yusoff, M. Vasilopoulou, D. G. Georgiadou, L. C. Palilis, A. Abate, M. K. Nazeeruddin, *Energy Environ. Sci.* **2021**, *14*, 2906.
[22] C. Luo, G. H. J. Zheng, X. J. Wang, F. Gao, C. L. Zhan, X. Y. Gao, Q. Zhao, *Energy Environ. Sci.* **2023**, *16*, 178.
[23] S. Y. Hou, Z. Ma, Y. L. Li, Z. W. Du, Y. Chen, J. B. Yang, W. You, Q. Yang, T. J. Yu, Z. F. Huang, G. M. Li, H. Y. Wang, Q. Y. Liu, G. Y. Yan, H. M. Li, Y. L. Huang, W. H. Zhang, M. Abdi-Jalebi, Z. P. Ou, K. Sun, R. Su, W. Long, *Adv. Funct. Mater.* **2024**, *34*, 2310133.
[24] H. Su, Z. Xu, X. L. He, Y. Y. Yao, X. X. Zheng, Y. T. She, Y. J. Zhu, J. Zhang, S. Z. Liu, *Adv. Mater.* **2024**, *36*, 2306724.
[25] L. Y. Lin, T. W. Jones, T. C. Jen Yang, X. Y. Li, C. C. Wu, Z. C. Xiao, H. J. Li, J. H. Li, J. W. Qian, L. Lin, J. Q. F. Shi, S. D. Stranks, G. J. Wilson, X. B. Wang, *Matter* **2023**, *7*, 1.
[26] H. Li, Z. Yan, M. Li, X. Y. Wen, S. Deng, S. S. Liu, W. C. H. Choy, L. J. Li, M.-Y. Li, H. F. Lu, *Chem. Eng. J.* **2023**, *458*, 141405.
[27] C. Zhang, H. Y. Li, C. Gong, Q. X. Zhuang, J. Z. Chen, Z. G. Zang, *Energy Environ. Sci.* **2023**, *16*, 3825.
[28] M. H. Wang, Y. F. Yin, W. X. Cai, J. Liu, Y. L. Han, Y. L. Feng, Q. S. Dong, Y. D. Wang, J. M. Bian, Y. T. Shi, *Adv. Funct. Mater.* **2021**, *32*, 2108567.
[29] X. B. Yuan, R. Li, Z. Xiong, P. Y. Li, G. O. Odunmbaku, K. Sun, Y. H. Deng, S. J. Chen, *Adv. Funct. Mater.* **2023**, *33*, 2215096.
[30] W. T. Wu, Q. Y. Chen, J. Cao, J. F. Fu, Z. L. Zhang, L. Chen, D. Rui, J. Zhang, Y. Zhou, B. Song, *ACS Appl. Mater. Interfaces* **2024**, *16*, 16340.
[31] Y. B. Gao, Y. J. Wu, Y. Liu, C. Chen, X. Bai, L. L. Yang, Z. F. Shi, W. W. Yu, Q. L. Dai, Y. Zhang, *ACS Appl. Mater. Interfaces* **2020**, *12*, 3631.
[32] J. J. Xue, R. Wang, K. L. Wang, Z. K. Wang, I. Yavuz, Y. Wang, Y. G. Yang, X. Y. Gao, T. Y. Huang, S. Nuryyeva, J. W. Lee, Y. Duan, L. S. Liao, R. Kaner, Y. Yang, *J. Am. Chem. Soc.* **2019**, *141*, 13948.
[33] D. Y. Luo, R. Su, W. Zhang, Q. H. Gong, R. Zhu, *Nat. Rev. Mater.* **2020**, *5*, 44.
[34] C. Tian, A. Sun, J. Liang, Z. Zhang, Y. Zheng, X. Wu, Y. Liu, C. Tang, C. C. Chen, *Small* **2023**, *19*, 2301091.
[35] C. Q. Ma, M.-C. Kang, S.-H. Lee, Y. L. Zhang, D.-H. Kang, W. Y. Yang, P. Zhao, S.-W. Kim, S. J. Kwon, C.-W. Yang, Y. Yang, N.-G. Park, *J. Am. Chem. Soc.* **2023**, *145*, 24349.
[36] H. Zhang, Q. W. Tian, W. C. Xiang, Y. C. Du, Z. T. Wang, Y. L. Liu, L. D. Liu, T. T. Yang, H. F. Wu, T. Nie, W. L. Huang, A. Najar, S. Z. Liu, *Adv. Mater.* **2023**, *35*, 2301140.
[37] X. J. Gu, W. C. Xiang, Q. W. Tian, S. Z. Liu, *Angew. Chem., Int. Ed.* **2021**, *60*, 23164.
[38] Y. Wang, J. X. Song, J. C. Ye, Y. Z. Jin, X. X. Yin, Z. Su, L. Hu, Y. Wu, C. F. Qiu, H. Wang, W. S. Yan, Z. F. Li, *Chem. Commun.* **2023**, *59*, 6580.
[39] Q. Jiang, Y. Zhao, X. Zhang, X. Yang, Y. Chen, Z. Chu, Q. Ye, X. Li, Z. Yin, J. You, *Nat. Photonics* **2019**, *13*, 460.
[40] X. D. Li, S. Fu, S. Y. Liu, Y. L. Wu, W. X. Zhang, W. J. Song, J. F. Fang, *Nano Energy* **2019**, *64*, 103962.
[41] D. Luo, W. Yang, Z. Wang, A. Sadhanala, Q. Hu, R. Su, R. Shivanna, G. F. Trindade, J. F. Watts, Z. Xu, T. Liu, K. Chen, F. Ye, P. Wu, L. Zhao, J. Wu, Y. Tu, Y. Zhang, X. Yang, W. Zhang, R. H. Friend, Q. Gong, H. J. Snaith, R. Zhu, *Science* **2018**, *360*, 1442.
[42] H. Zhu, K. Miyata, Y. Fu, J. Wang, P. P. Joshi, D. Niesner, K. W. Williams, S. Jin, X. Y. Zhu, *Science* **2016**, *353*, 1409.
[43] C. W. Li, X. M. Wang, E. B. Bi, F. Y. Jiang, S. M. Park, Y. Li, L. Chen, Z. W. Wang, L. W. Zeng, H. Chen, Y. J. Liu, C. R. Grice, A. Abudulimu, J. Chung, Y. M. Xian, T. Zhu, H. G. Lai, B. Chen, R. J. Ellingson1, F. Fu, D. S. Ginger, Z. N. Song, E. H. Sargent, Y. F. Yan, *Science* **2023**, *379*, 690.
[44] M. G. Li, Y. Peng, W. J. Pan, Z. Z. Wang, J. W. Zong, Z. Zhu, L. Zhao, H. Gao, R. F. Chen, *ACS, Appl. Enegry Mater.* **2023**, *6*, 4150.
[45] Y. Li, L. Liu, C. Zheng, Z. Liu, L. Chen, N. Yuan, J. Ding, D. Wang, S. Liu, *Adv. Energy Mater.* **2022**, *13*, 2203190.
[46] X. D. Li, H. Yang, A. C. Liu, C. Y. Lu, H. B. Yuan, W. X. Zhang, J. F. Fang, *Energy Environ. Sci.* **2023**, *16*, 6071.

[47] X. Q. Jiang, B. Q. Zhang, G. Y. Yang, Z. M. Zhou, X. Guo, F. S. Zhang, S. T. Yu, S. W. Liu, S. P. Pang, *Angew. Chem., Int. Ed.* **2023**, *62*, 202302462.
[48] R. Wang, J. Xue, K. Wang, Z. Wang, Y. Luo, D. Fenning, G. Xu, S. Nuryyeva, T. Huang, Y. Zhao, J. L. Yang, J. Zhu, M. Wang, S. Tan, I. Yavuz, K. N. Houk, Y. Yang, *Science* **2019**, *366*, 1509.
[49] Q. Zhou, Y. Gao, C. Cai, Z. Zhang, J. Xu, Z. Yuan, P. Gao, *Angew. Chem., Int. Ed.* **2021**, *60*, 8303.
[50] H. Zhang, Y. Z. Wu, C. Shen, E. P. Li, C. X. Yan, W. W. Zhang, H. Tian, L. Y. Han, W.-H. Zhu, *Adv. Energy Mater.* **2019**, *9*, 1803573.
[51] X. Zheng, B. Chen, J. Dai, Y. Fang, Y. Bai, Y. Lin, H. Wei, X. C. Zeng, J. Huang, *Nat. Energy* **2017**, *2*, 17102.
[52] F. Z. Li, X. Deng, F. Qi, Z. Li, D. J. Liu, D. Shen, M. C. Qin, S. F. Wu, F. Lin, S.-H. Jang, J. Zhang, X. H. Lu, D. Y. Lei, C.-S. Lee, Z. L. Zhu, A. K.-Y. Jen, *J. Am. Chem. Soc.* **2020**, *142*, 20134.
[53] J. Jiang, M. Xiong, K. Fan, C. Bao, D. Xin, Z. Pan, L. Fei, H. Huang, L. Zhou, K. Yao, X. Zheng, L. Shen, F. Gao, *Nat. Photonics* **2022**, *16*, 575.
[54] C. Q. Ma, M.-C. Kang, S.-H. Lee, S. J. Kwon, H.-W. Cha, C.-W. Yang, N.-G. Park, *Joule* **2022**, *6*, 2626.
[55] C. V. Thompson, *J. Appl. Phys.* **1985**, *58*, 763.
[56] X. Zheng, Y. Hou, C. Bao, J. Yin, F. Yuan, Z. Huang, K. Song, J. Liu, J. Troughton, N. Gasparini, C. Zhou, Y. Lin, D.-J. Xue, B. Chen, A. K. Johnston, N. Wei, M. N. Hedhili, M. Wei, A. Y. Alsalloum, P. Maity, B. Turedi, C. Yang, D. Baran, T. D. Anthopoulos, Y. Han, Z.-H. Lu, O. F. Mohammed, F. Gao, E. H. Sargent, O. M. Bakr, *Nat. Energy* **2020**, *5*, 131.
[57] J. Li, L. Zuo, H. Wu, B. Niu, S. Shan, G. Wu, H. Chen, *Adv. Funct. Mater* **2021**, *31*, 2104036.
[58] J. H. Ren, T. H. Liu, B. C. He, G. B. Wu, H. Gu, B. Z. Wang, J. L. Li, Y. L. Mao, S. Chen, G. C. Xing, *Small* **2022**, *18*, 2203536.
[59] M.-J. Choi, J.-W. Lee, H. W. Jang, *Adv. Mater.* **2023**, *36*, 2308827.
[60] Y. Zhang, T. Kong, H. Xie, J. Song, Y. Li, Y. Ai, Y. Han, D. Bi, *ACS Energy Lett.* **2022**, *7*, 929.
[61] M. I. Saidaminov, J. Kim, A. Jain, R. Quintero-Bermudez, H. R. Tan, G. K. Long, F. R. Tan, A. Johnston, Y. C. Zhao, O. Voznyy, E. H. Sargent, *Nat. Energy* **2018**, *3*, 648.
[62] J. P. Wu1, S.-C. Liu, Z. B. Li, S. Wang, D.-J. Xue, Y. Lin, J.-S. Hu, *Natl. Sci. Rev.* **2021**, *8*, nwab047.
[63] Y. Y. Meng, Y. L. Wang, C. Liu, P. Y. Yan, K. X. Sun, Y. H. Wang, R. J. Tian, R. K. Cao, J. T. Zhu, H. N. Do, J. F. Lu, Z. Y. Ge, *Adv. Mater.* **2023**, 2309208.
[64] D. Y. Ma, W. L. Li, X. J. Chen, Z. Yang, J. Zhao, Z. Y. Yang, Y. Zhang, Z. G. Chi, *Small* **2021**, *17*, 2100678.
[65] A. K. Ojha, S. K. Srivastava, B. P. Asthana, R. K. Singh, *J. Raman Spectrosc.* **2007**, *38*, 159.
[66] L. Jiang, J. Lu, S. R. Raga, J. Sun, X. Lin, W. Huang, F. Huang, U. Bach, Y.-B. Cheng, *Nano Energy* **2019**, *58*, 687.
[67] G. Divitini, S. Cacovich, F. Matteocci, L. Cina, A. D. Carlo, C. Ducati, *Nat. Energy* **2016**, *1*, 15012.